LUND UNIVERSITY

# Photoelectron Spectroscopy using high repetition rate attosecond pulses

Lisa Rämisch

Thesis submitted for the degree of Bachelor of Science
Project duration: 2 months

Supervised by Miguel Miranda and Mathieu Gisselbrecht

Department of Physics

Division of Atomic Physics

05-2017

## Acknowledgements

Research work is often team work. Therefore, I would first of all like to thank the whole attosecond physics group for integrating me into their multicultural team of passionate scientists and coffee drinkers. I could always count on you when I had a question. Most importantly, I'd like to thank my supervisors for their guidance. Miguel for his dry humor and help with anything related to labview and RABBITT. Now I know why people call you the labview king. Mathieu for sharing his extremely big and impressive knowledge with me, for always motivating me, for awakening my curiosity and for keeping my french language skills up to date. I dedicate this work to my family who has brought me to where I am today through their constant support, trust and advice.

**Abstract**

In attosecond physics, pump-probe experiments have been a promising tool to study the fundamental light-matter interaction process of photoionization. In this context, photoelectron spectroscopy is used to spatially and temporally characterize the ejected photoelecron. Low repetition rates can be limited in resolution by space-charge effects [1] and measurement statistics which can be reduced by high repetition rate measurement of photoelectron spectra.

This thesis presents how a high speed digital signal processing card is implemented together with a programmed application software to measure high repetition rate photoelectron spectroscopy. In order to analyze the acquisition conditions and the spectrum generation, the card is tested with a $1kHz$ laser system. We measure the travel time (time-of-flight) of photoelectrons from the moment of ionization until the moment of detection and further convert this quantity to kinetic energy. The results show that both time-of-flight and kinetic energy photoelectron spectra can be measured with the established setup. We corrected a trigger offset to better resolve sidebands created during the pump-probe experiments. We understood that the peak detection function provided by the graphical programming software Labview requires specific input parameters to better resolve the photoelectron time-of-flights and that the current duty cycle needs to be adjusted for high repetition rate measurements. The implementation of the acquisition cards Zero-Suppress mode remains an important feature to reduce the amount of data flow.

# Contents

# Abbreviations

**EWP** = electron wave packet
**NIR** = near Infrared
**XUV** = ultraviolet
**MHz** = MegaHertz
**kHz** = kiloHertz
**TOF** = time-of-flight
**MBES** = magnetic bottle electron spectrometer
**AP** = Application Software
**GS** = Giga Samples
**DSPC** = Digital Signal Processing Card

# 1 Introduction and Scientific Background

## 1.1 Motivation

The first generation of attosecond pulses in 2001 [2, 3] laid the foundation for real time photoelectron spectroscopy which enables scientists today to resolve the process of photoionization in space and time [4]. The study of the time evolution of a photoelectron[5] represents an important advancement in fundamental research as it provides better insight into light-matter interactions [6].

The attosecond physics research group in Lund and other attosecond research groups investigate photoemission delays during photoionization by measuring electron kinetic energy spectra using pump-probe experiments [7]. With the setups in the attosecond laboratories at the atomic physics division, laser pulses are delivered at low repetition rates from 10 Hz to 1 kHz [4]. Currently, those repetition rates can limit the statistics of the measurement and the application of attosecond light source to gas phase. Indeed, on a solid target, the high amount of photons per pulse can lead to space charge effects[1]. Consequently, the kinetic energy resolution is strongly deteriorated as photoelectrons repel each other due to the Coulomb interaction.

In order to improve the statistics without drastically increasing the acquisition time or affecting the kinetic energy resolution, the motivation of this thesis is to utilize a laser at a high repetition rate, of the order of $10^2$ kHz. The laser should generate attosecond pulses to ionize gases and to measure photoelectrons with a high-speed acquisition card. This should allow a 200 times higher measurement rate. Eventually, in the long term, photoelectron spectroscopy at high repetition rates benefits applications, in - but not limited to - surface and structure studies of materials, in the study of materials conductivity [7] and the study of molecules in biology [8].

## 1.2 Photoionization

All experiments conducted in this thesis are based on the light-matter-interaction process of photoionization. This section provides an overview of how an electron wave packet (EWP) can be characterized temporally during photoionization and the quantities which are used throughout the thesis.

Photoionization is related to the transition of an atom to an ion by emitting an electron after absorption of a photon [9].

$$h\nu + A \rightarrow A^+ + e^- \tag{1}$$

This process is energetically possible if the energy of the incoming photon exceeds the binding energy of the electron. This process was first explained by Einstein [10] in the case of the photoelectric effect showing that the kinetic energy of the electron after ionization

corresponds to the difference in photon and binding energy $E_{kin} = hv - E_{binding}$. Due to the broadband nature of an attosecond pulse an EWP is created upon photoionization. In the time domain, the EWP moves from a bound state $\varphi_i$ to many continuum states $\varphi_k$ [5]. The emitted EWP will experience a delay during photoionization[11, 6] due to the ionic attractive potential $V \neq 0$ [12], which offsets the electron trajectory with respect to a free electron with no encountered potential $V = 0$. An attractive potential leads to a transmitted wave which is delayed relative to a free electron wave [12].

In order to define the time delay of the EWP during a pump-probe experiment, we briefly present the quantum mechanical description of the photoionization which is based on scattering theory [11]. Here the collision between particles occurs between the photon and the atom [13]. The photon can be treated as a classical electric field $E(t)$, and the Hamiltonian which characterizes the interaction between the photon and the bound state is defined as $H_i = zE(t)$. The EWP at position $\mathbf{r}$ and time $t$ is defined by the sum over all outcoming (-) continuum wave functions $\varphi_{\mathbf{k}}^{(-)}$ at an energy $\epsilon_k$ with a probability density $a(\mathbf{k}, t)$ [11]:

$$\Psi(\mathbf{r}, t) \; = \int d\mathbf{k}\, a(\mathbf{k})\, \varphi_{\mathbf{k}}^{(-)}(\mathbf{r})\, e^{-i\epsilon_k t} \tag{2}$$

The probability density to find the photoelectron wave packet in a given state $\mathbf{k}$ of energy $\epsilon_k$ from an initial state of energy $\epsilon_i$ is given by:

$$a_i(\mathbf{k}) = -i\, M_i(\mathbf{k}) \int_{-\infty}^{\infty} dt' E(t) e^{i(\epsilon_k - \epsilon_i)t'} \tag{3}$$

where $M_i(\mathbf{k}) = \langle \varphi_{\mathbf{k}}^{(-)} | \hat{H}_i | \varphi_i \rangle$ is the dipole matrix element which characterized the transition from $\varphi_i$ to $\varphi_{\mathbf{k}}^{(-)}$ and the integral corresponds to the Fourier transform of the electrical field E(t) at the energy difference $\epsilon_k - \epsilon_i$. In other words, it describes the electrical field in the frequency domain [11]. The time delay of the EWP $\tau_W^i$ can be obtained by partially deriving the argument of the transition matrix $M_i(\mathbf{k})$ with respect to the energy of a continuum state $\epsilon_k$:

$$\tau_W^i(\epsilon_k, \Omega_k) = \frac{\partial}{\partial \epsilon_k}\, arg[M_i(\mathbf{k})] \tag{4}$$

The above definition is**?** important as high-repetition rate photoelectron spectroscopy can eventually be employed to study the photoemission time delay. During an experiment, the EWP is probed with an NIR laser field. The interaction between the EWP and the NIR laser field is responsible for another delay $\tau_{CC}^i$ [14]. Hence, the measured photoemission delay is equal to the sum of both above defined delays :

$$\tau_{EWP}^i = \tau_W^i + \tau_{CC}^i. \tag{5}$$

The outgoing photoelectron wave function at different energies $\epsilon_k$ is the main parameter which is detected in this thesis by the apparatus described in 2.1.3.

## 1.3 This work

This thesis paves a path for high repetition rate measurements of photoelectron spectra. Researchers at the attosecond physics research group in Lund aim to implement pulses at repetition rates at the order of MHz in order to minimize the side effects of low repetition rates which decrease the signal-to-noise ratio and in order to increase measurement statistics [15].

For now, there is no digitizer card installed and programmed for the use of high repetition rate measurements in the 200 kHz laboratory in Lund. This thesis work consists of developing an application software (AP) in Labview which configures a high speed acquisition card, accumulates and digitizes analog data and further processes this data to a Time-of-flight (TOF) and energy spectrum. The long term aim is to use this card for high repetition rate measurements in the megahertz laboratory. This AP has been implemented with the high speed digital signal processing card (DSPC) $U1084A$ containing the DGS firmware [16]. The advantage of this card is its high-speed data acquisition with a sampling rate of up to $4GS$ per second and a $512MB/s$ processing memory [16]. For repetition rates at $200kHz$, high speed analog-to-digital converters are advantageous to withstand the data flow at every $\mu s$. The card is tested with the old MBES setup (see section 2.3) and with the laser in the attosecond laboratory at Lund university. The cards settings are optimized to measure photoelectron spectra.

In the beginning of the thesis work, the experimental set-up is presented and the measurement tools are described in more detail. Furthermore, the application software programmed in Labview is derived and explained.

In the analysis, time-of-flight (TOF) and kinetic energy spectra and the acquisition process are presented and analyzed by looking at hardware and software aspects. Most importantly, it is discussed whether the acquisition method together with the software program is suitable for measurements at $200\,kHz$ repetition rate and what improvements need to be made in order to make those measurements possible in the future.

# 2 Methods

This section presents the tools used to measure photoelectron spectra. The experiments in this thesis were conducted at the attosecond laboratory in the atomic physics division at Lund university. The first experimental part explains how the photoelectrons are generated and how the analog signals related to the detection of the electrons are analyzed. In the second part, the digital data accumulation with the programmed acquisition card $U1084A$ by Keysight technologies is demonstrated.

## 2.1 Experimental Set-up

At the origin of photoelectron spectroscopy is the laser apparatus which generates pulses in the near infrared region (NIR) centered at a wavelength of $800nm \pm 50nm$ with frequency $\omega_{NIR}$ [14]. The laser pulses are defined by their repetition rate $f_{rep}$ and their pulse energy $E_p$ [17].

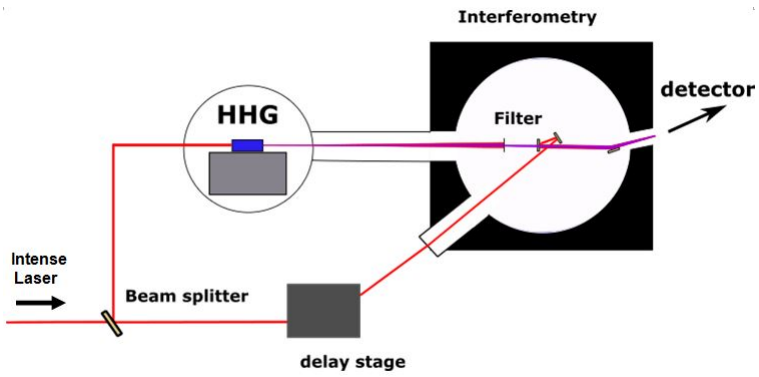


Figure 1: Illustration of the experimental pump-probe setup. The propagation of the laser beam is illustrated in red. The High order Harmonic generation (HHG) chamber responsible for the generation of attosecond pulses is depicted in blue. After the interferometric chamber where attosecond pulses are filtered and recombined with the NIR laser, both light fields are re-focused into another chamber to measure real time photoelectron spectroscopy.

### 2.1.1 Attosecond Pulses

The first tool is an attosecond pulse train in the extreme ultraviolet region (XUV) of the electromagnetic spectrum; $\lambda < 100\,nm$ . An attosecond pulse train (APT) is defined as a succession of constantly separated light pulses with a duration at the order of $10^{-18}$ seconds.

APTs are the result of high-order harmonic generation (HHG), which is obtained by focusing an intense femtosecond driving laser. For an intensity of $10^{14}\,W/cm^2$, the laser can generate efficiently odd harmonic orders in the XUV region [15] which is explained by a semiclassical, so called "three step model" ( see figure 2) [18], first introduced in 1993 [4].

This model approximates the motion of an electron in a strong laser field. In the first step (I), an EWP from the outer shell of an atom is tunneling through the Coulomb potential of the atom. Secondly (II), the EWP is driven and accelerated by the laser-electron interaction until thirdly (III), the EWP is recaptured by its parent ion where it deexcites by emitting a photon of energy $\hbar\omega$ [18]. The above explained three steps occur every half laser cycle and result therefore in an ATP where every pulse is separated by half the laser period of 1.3 fs. This corresponds to a separation of $2\hbar\omega_{NIR}$ between photon peaks [5].

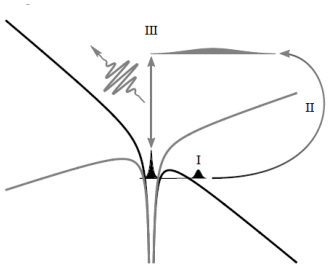


Figure 2: Representation of the three step model: I: electron tunneling, II: electron acceleration, III: electron recapture [18].

Figure 1 indicates how the NIR pulsed beam (in red) is focused onto a gas chamber (in blue) with a focus diameter of several micrometers. There will be a certain amount of the initial NIR field traveling through the gas chamber without generating higher harmonics. To prevent this laser field from further interacting with matter, it is blocked by a filter (see figure 2) which only allows the harmonic field to pass through [18]. When the XUV pulses are absorbed with atoms of a gas medium, those atoms are ionized. In that case, only the end product of the photoionization can be measured such as the yield of the photoelectron signals [5]. In order to characterize the electron temporally, a cross-correlation measurement is required.

### 2.1.2 RABBITT technique

The 'reconstruction of attosecond harmonic beating by interference of two-photon transitions (RABBITT)' technique is a cross-correlation technique which utilizes the interferometric signal between the induced photoelectrons and the NIR Laser field. In the interferometry chamber, the NIR beam is recombined with the APT pulse train, so it is possible to control the overlap in time and space between both fields[18]. A delay stage controls the separation in time $\tau$ between between both overlapping pulses. Both fields are then focused into a gas jet at the center of an electron spectrometer (see below).

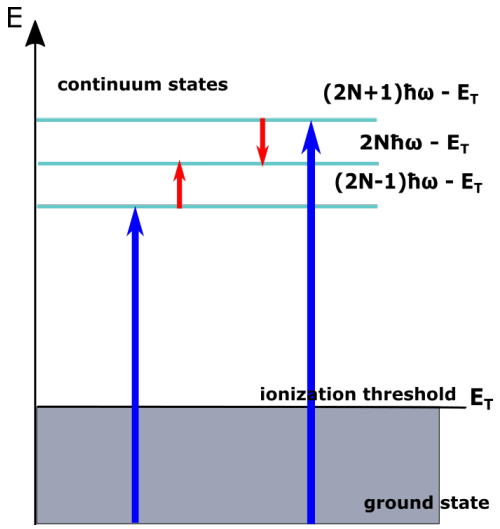


Figure 3: Visualization of the two color ionization process. The electron is transferred from the ground to continuum states (light blue) above the ionization threshold $E_T$

The XUV pulse initiates the ionization process and the electron moves to a continuum state of energy $2(N+1)\,\hbar\omega_{NIR} - E_T$ (blue arrow figure 3). The NIR pulses then interact with the photoelectron. Depending on the interaction, one NIR photon is either absorbed or emitted (red arrows in figure 3). The result of this process known as two-color photoionization [5] are so-called sidebands. They appear at photoelectron energies initiated by even orders of the NIR field energy $E_{even} = 2N\,\hbar\omega_{NIR} - E_T$.

Second order perturbation theory describes how the signal of the sidebands varies with three different time delays[18]:

$$S = A + Bsin(\Delta\phi - \Delta\phi_{harm} - \Delta\phi_{EWP}) = A + Bsin(2\omega(\tau - \tau_{harm} - \tau_{EWP})) \quad (6)$$

$\tau_{EWP}$ is the sum of two delays which both characterize the photoemission delay explained in section 1.2.1. The delay between harmonics $\tau_q^{XUV}$ can experimentally be omitted and the delay between the XUV and the NIR pulses $\tau$ is controllable. $\tau_{EWP}$ can then be determined experimentally [11].

### 2.1.3 Electron spectrometer and detection

For the photoelectron detection in this thesis a magnetic bottle electron spectrometer (MBES) of length L is implemented. The overlapping NIR and harmonics fields interact with a gas that we want to study. The interaction region is located at the entrance of the MBES ( see figure 4a). There the photoelectrons are first collected by a strong permanent magnet of $1T$ and then further directed onto the end of the MBES tube by solenoid magnetic field lines B. Both magnets parallelize the electrons momentum relative to the magnetic field lines in order to detect them by the micro-channel plates detector (MCP) (see figure 4 below). The MBES apparatus is kept under vacuum to avoid interactions between the traveling electron and surrounding molecules.

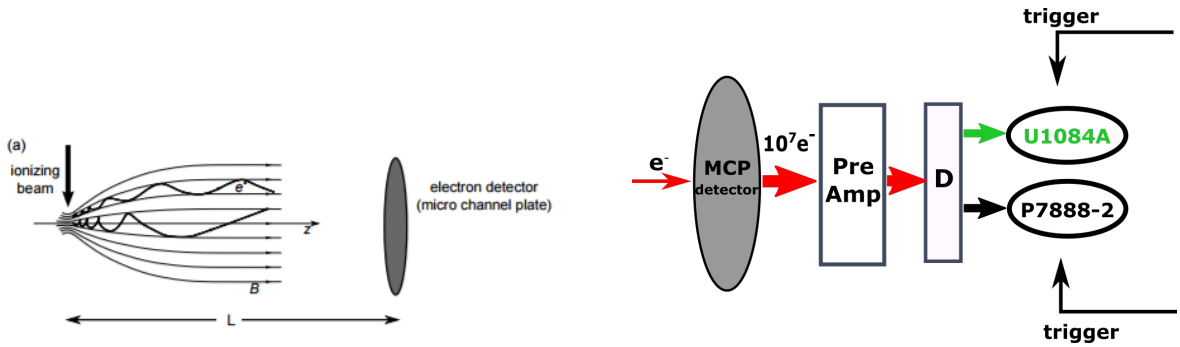


(a) (b)

Figure 4: (a) Illustration of photoelectron trajectories in the MBES from ionization to the detector (MCP) (b) Illustration of electronic accumulation from the MCP detector to the pre-amplifier(Pre-Amp) and the discriminator D. Both digital processing cards $U1084A$ and $P7888-2$ accumulate the signal after the reception of a trigger.

In the MCP, the signal related to an electron is amplified by an avalanche process,

where electrons knock out each other in each micro channel. A typical gain of $10^7 - 10^9$ can be achieved (see figure 4b). The signal is further pre-amplified by a factor of $10^2$ in the pre-amplifier (Pre-Amp), then sent to a discriminator which recognizes the peak and creates an inverted rectangular pulse of $-800\,mV$ after NIM-standard[19] at the position of the pulse peak. This digital signal is then transported through two separate wires to the digitizer cards $U1084A$ and $P7888 - 2$. In order to determine the time that it takes for the electron to travel from the ionization chamber to the MCP, known as time-of-flight (TOF), the time difference between two trigger events should be measured [14]. The first one, used as a reference time, is given by the NIR laser pulses which hit a photodiode and thereby induce a current. This current is strong enough to be measured directly by the digitizer card without amplification. The second trigger corresponds to the measured photoelectron charge pulse leaving the discriminator. In the thesis, the TOF is measured and used to construct the photoelectron spectrum by calculating the electron kinetic energy acquired along the tube length L:

$$E_K = \frac{1}{2}\, m_e \left(\frac{L}{TOF}\right)^2 \tag{7}$$

L represents the length from the ionization point to the MCP detector. For the length, the curvature of the electron in the beginning of its flight is negligible since the radial and the tangential component of the velocity are assumed to be decoupled. Relativistic terms in the energy calculation are negligible since the electrons velocity is at the order of $10^6 m/s$.

## 2.2 Acquisition System

The main tool used to acquire the photoelectron spectrum is a high-speed digital signal processing card (DSPC) named $U1084A$ and provided by Keysight Technologies with serial number 61066. It operates at a band-path of $1GHz$ and codes the amplitude of the signal with 8 bits [16].

### 2.2.1 Hardware installation

The DSPC $U1084A$ is connected to a Personal Component Interconnect Express (PCIe) input bus [16] which is installed on the main computer printed wire board (see appendix A). The hardware can be accessed by the PCI resource name "PCI::INSTRn" which uses the order n of found instruments with PCI connection (step A figure 5) or the connection can be established by the PCIe instrument bus and slot connection (see appendix A). The use of a PCIe can increase the data throughput to a conventional PCI connection and allows for data sent at $520MB/s$. The two inputs used in this thesis are the channel 1 which is connected to the discriminator and the trigger input which is connected to the photo diode (see [16]).

### 2.2.2 Acquisition Interface

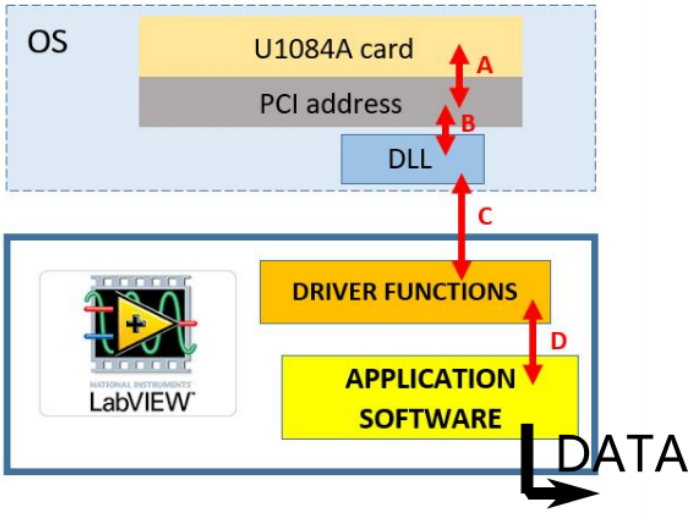


Figure 5: Illustration of acquisition environment: Step A: The card is accessible via the operating system and is identified through its PCIe address. Step B and C: A package of shared libraries (DLL) in the operating system provides driver functions for the labview application software. Step D: An application software uses the driver functions and extracts the relevant peak data to construct TOF and energy spectra.

Figure 5 illustrates how the application software program does acquire data. Through one of two input channels, the card receives an analog signal from the MCP and converts it to a digital signal defined by 0 (low) and 1 (high) digits. The digitization process is required to further numerically work with the signal.

The card is installed in the operating system (OS) which in our case is Windows 10 64-bit. Without the AP, the pulses from the discriminator cannot be accessed. Neither can the card be controlled, any settings of the card be modified nor can the user verify the data output through visualization. The AP is programmed in LABVIEW 2015 $32-bit$. It identifies and connects to the card via the PCI address. Only when the card is initialized and its instrument ID is received, it can be configured and used. The next step of the interface is then to use driver functions provided by Keysight Technologies [20] which are connected to a dynamic link library (dll) (step B). A dll contains different shared function which can be accessed while the software is running [21]. The driver functions need to be programmed in the application software in order to configure the card and to access the digitized data (step D).

#### Configuration

Before any data can be collected, the accumulation settings must be configured. Those include for example the trigger signal in mV, the vertical voltage range of the signal, the sample resolution as well as memory space settings. The $U1084A$ card works in two

operation modes. Before accumulating data in either one of them, the operation mode together with all necessary parameters must also be initiated.

**Data Accumulation**

The data acquisition in both cases relies on an external trigger signal - connected to trig. input (see [16]) - which is provided by the NIR Laser signal captured by a photodiode. If the laser is switched off, a software trigger provides a backup trigger signal. With every positive edge of the trigger signal, a set number of samples is acquired at a pre-set time interval .

If the device operates in mode 0, the card saves all data points in a data array in memory and visualizes them. The visualization of the data is important as it helps to verify the correct configuration settings. For each consecutive trigger event, the raw data array is renewed by the current data. Therefore, to keep all data points, the processing steps to obtain the spectrum are executed right after each accumulation.

The photoelectron spectrum is created by software through a labview peak detection function. Above a certain threshold, a quadratic function is fit to every peak point including a bandwidth of $\pm width$ points. The peak detection function returns both the intensity of the peak as well as its measurement time index relative to the trigger event. For all peaks, those time values are collected and added onto a histogram. Eventually, after an important number of photoelectron peak detections, the spectrum is created. The overall algorithm occurs in sequence and the data array is renewed with every accumulation, the peak detection takes place after every trigger event.

### 2.2.3 Accumulation Modes

There are two ways to acquire photoelectron signals with the DSPC $U1084A$: either in the normal acquisition mode (0) which displays all raw data as an oscilloscope or in the Zero-Suppress Mode (7). The firmware DGS of the $U1084A$ digitizer contains the Zero-Suppress acquisition process which allows to increase the acquisition speed by lowering the data storage [22]. This mode is advantageous as it only stores relevant data for the signal processing operations . The main idea is to divide the signal into gates [20] in which a user-defined threshold value is applied. Furthermore, the memory is virtually di-

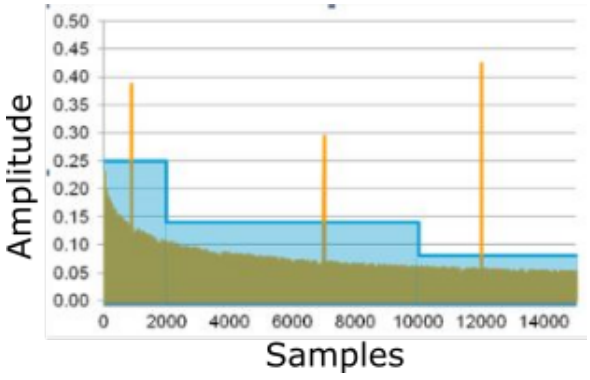


Figure 6: Representation of gate separation and threshold application in the Zero-Suppress Mode ( ref: [22])

vided into segments. Those segments should show repetitive pattern. Eventually, the data output array stores meta-data describing both the segments and the gates as well as raw data. The $8 - bit$ unsigned raw data, which only contains values below the given threshold, is stored as signed 8-bit values with the help of the two-complements-method [20].

The labview processing speed at the level of labview benefits from the Zero-Suppress mode since it has to run through less data points in order to filter out the relevant photoelectron peaks. Moreover, Labview only supports 2 to 4 GB data storage [23]. Therefore the risk of a malfunctioning software programm is lowered at this mode 7. At high-repetition rates, thus at lower pulse energy, not all laser pulses might lead to a photoionization event and applying thresholds to suppress irrelevant data is therefore beneficial.

# 3 Results and Discussion

The studies in this thesis were performed with the laser system in the attosecond laboratory at the atomic physics department. The radiation is first produced by a Ti:Sapphire mode locked oscillator and then runs through a chain of amplification processes until the final pulses achieve an energy of $5\,mJ$, at a duration of $20\,fs$ and at repetition rate of $1\,kHz$ [18]. These laser pulses lie in the near infrared (NIR) region and are centered at a wavelength of $800\,nm \pm 50\,nm$ [14]. The $1\,kHz$ laser setup is chosen as an alternative to the 200 kHz laser setup in the $200kHz$ laboratory.

Neon gas atoms are used to construct both TOF and KE spectra. Neon (atomic number $Z = 10$) is a noble gas with the electronic configuration $1s^2 2s^2 2p^6$. Since it is a close shell atom, neon is not chemically reacting and therefore advantageous to use in our experiments [24]. The spectra obtained with the newly programmed DSPC $U1084A$ are compared to the spectra measured with the $P7888-2$ fastcomtec acquisition system currently used for research in the $1\,kHz$ setup. Four different aspects, the trigger signal, the built-in peak detection labview function, the energy spectrum calibration and the acquisition duty cycle, and their influence on the acquisition are discussed during the presentation of results.

For the analysis of those aspects, it is important to note that both DSPCs measure pulses which are provided by the NIM standard and are therefore supposed to be identical in shape and amplitude [19]. An example of how the acquisition interface visualizes the digital signal from the discriminator is given below:

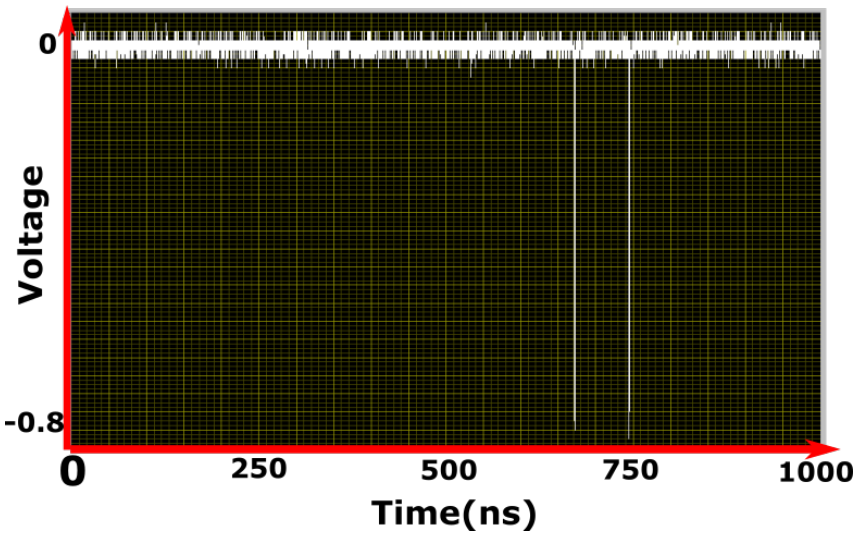


Figure 7: Visualization of outgoing rectangular peaks from the discriminator created with the NIM standard. TOF is shown in seconds on the x-axis and the amplitude of the pulse in arbitrary units on the y-axis. Each pulse ccorresponds to an amplitude of -800 mV and a width of several nanoseconds [19].

## 3.1 Trigger

The following section demonstrates the effect on a trigger offset on the resolution of photoelectron spectra.

For the measurements, the trigger signal is provided by the NIR laser signal. The pulses are likewise at a repetition rate of $1\,kHz$ and deliver a positive signal at an amplitude of around $250\,mV$ which needs to be set as a "Trigger level 1" (see appendix D1). The time resolution for the TOF spectra is chosen to be $1ns$ and the acquisition window is divided into 10000 points, i.e. the acquisition window ranges from zero to ten microseconds. The range of the signal is chosen to be $1-2V$. The data accumulation is done in normal acquisition mode 0. The peaks are detected with a Labview peak detection function using a sampling width of $3-10$ sample points and a threshold of 27 corresponding to an arbitrary amplitude indication on the y-axis.

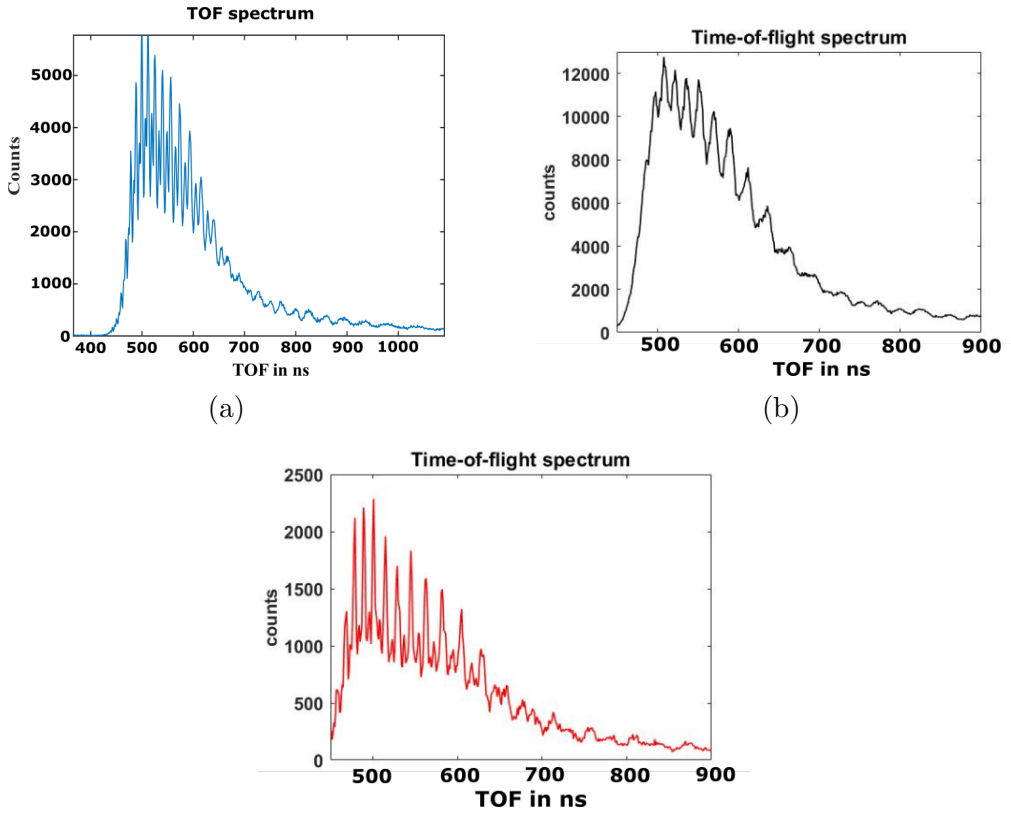


(a) (b) (c)

Figure 8: TOF spectra of neon acquired with different acquisition systems before and after correction for the trigger offset: (a) TOF spectra acquired with the old acquisition card and a bin width of $1ns$ (b) Spectra acquired with the new digitizer using a bin width of $1ns$ (c) Spectra acquired with the $U1084A$ digitizer after correction for the trigger offset

The graphs shown in figure 8 present the number of photoelectrons as a function of their TOF in seconds. The fastest photoelectrons are first at the MCP with the lowest TOF and correspond to the first peaks in all subfigures.

By comparing figure 8a and 8b, one can clearly see that the number of resolved

peaks with the new digitizer card is much lower than the number of peaks measured with the old card. In figure 8a, while the peaks of higher intensities are related to the ionization by the APT, the peaks of lower intensities in between are the sideband signals $S_q$ (see equation 7). Those sidebands are expected to be induced by two-color photoionization in the perturbative regime (see section 2.1.2) and appear at weaker intensities of around $20 - 50\%$ of the main ones. For both acquisition systems, the fastest photoelectron is indicated to take $500 \pm 30ns$ and the slowest around $980 \pm 30\,ns$. By having a closer look at the first peaks in figure 8b made with the digitizer, we can only see broad peaks related to the ionization process. These peaks are clearly resolved and correspond exactly to the values measured with the former $P7889 - 2$ digitizer. However, the sidebands $S_q$ are not visible. It can be concluded that their missing visibility is not caused by less photoelectron counts since the data of the new card in figure 8b reaches up to 13000 photoelectron peaks compared to only 6000 measured by the old card in figure 8a.

The missing sidebands ought to be caused by a problem during the accumulation process which is either caused by hardware or by software. We first check the first data point index which is provided by the data accumulation driver function [25] and which should correspond to zero. However, by verifying its value, we discovered that it is greater than zero which implies that the first data point (see fig.9) $i_{start}$ is taken with an offset "hoffset" relative to the trigger as shown in figure 9 below.

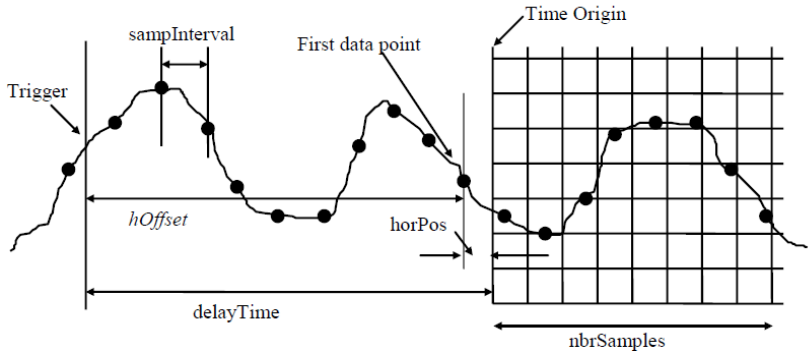


Figure 9: Representation of the "offset" of the first data point with respect to the detected trigger pulse [source: [20]]

This offset is corrected by shifting all data points by the value of $i_{start}$ to the left so that the data accumulation - indicated by the grid in fig. 9 - starts right after the trigger line.

## 3.2 Peak detection

Even after the trigger offset correction, the resolution or visibility of the sideband peaks remains a major difference in between the old and new card in figure 8a and 8c respectively. Though a complete analysis could not be carried out, we want to understand which software settings are most suitable to provide the best peak resolution. For that purpose,

spectra with different input parameters for the Labview peak detection function have been created and the sideband resolutions have been compared.

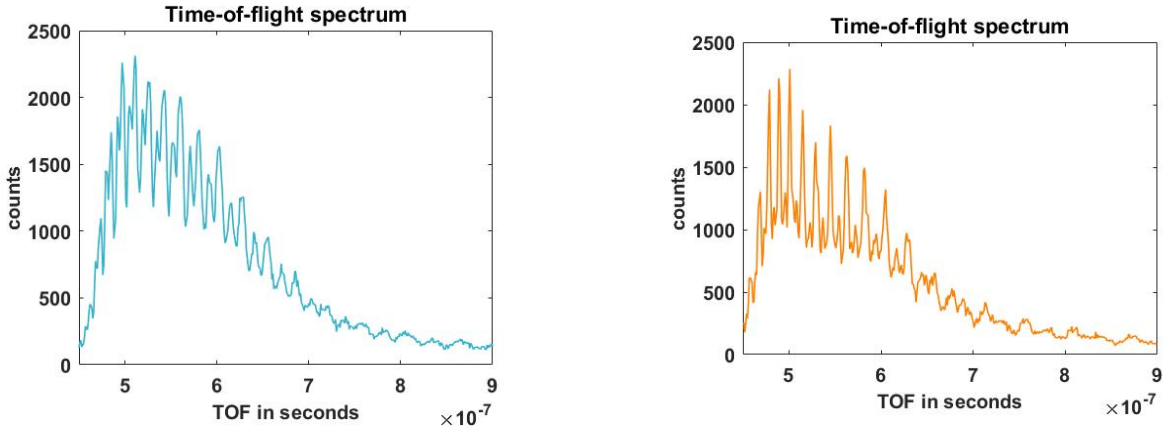


(a) (b)

Figure 10: TOF spectra made after trigger offset correction with the $U1084A$ digitizer: (a) spectrum made using Labview peak detection with a width value of 8 sample points and 450 histogram bins each of $1ns$ (b) spectrum made using Labview peak detection with a width value of 10 and 400 histogram bins each of 1.125 ns

Figure 10a and 10b show different TOF spectra with different input parameters. Those are the number of samples taken into consideration when looking at the $S_q$ peak amplitudes and their distance from the peak to the nearest minimum, the sidebands $S_q$ are better resolved in figure 10a. In that case, the width for the quadratic fit in the Labview peak detection has been chosen as 8 sample points and the bin width as $1.125\,10^{-9}s$. In figure 10b the Labview peak detection width encloses 10 sample points with a histogram bin width of $1\,ns$.

It appears that a chosen peak detection width input of less than 10 sample points is more suitable since the quadratic fit encloses only the nearest sample points to each peak. The histogram bin time range does not seem to be the cause of missing resolution since the histogram bin width of the old card equals $1\,ns$ as in figure 10b. Therefore, as the photoelectron count statistics for the old card in figure 8a are double as high as in figure 10a and b, the sidebands might start appearing higher in amplitude for greater count statistics on the order of $10^4$ for example. It might be possible that the hardware at this level is not responsible for missing statistics in the peak detection process, but the Labview peak detection function since the incoming pulses are identical for both acquisition cards.

In order to perform a complete analysis, the raw data of every accumulation window after each trigger event must be saved. This option should be included in the acquisition interface since it would allow us to test different parameters for the Labview peak detection. Moreover, other peak detection mechanisms such as the identification of $f'' = 0$ at each peak could be implemented. It would allow us to reconstruct and study the histogram with different parameters.

## 3.3 Calibration

In this section, the energy spectra are processed from the TOF values (see equation 7). It is discussed how the energy calibration limits the results.

The first ionization for neon occurs when an electron from the $2p^6$ shell is ejected. The kinetic energy values are calculated right after obtaining the TOF values. Both spectra can then be obtained by peak detection or alternatively the energy spectra can rely on the conversion from the TOF spectra : $\frac{dN}{dE} = \frac{dt}{dN}\frac{dE}{dt}$. In the acquisition system made, we chose the first method to create the kinetic energy histogram.

As the KE spectrum is created online right after the TOF spectrum for each trigger event, the data accumulation settings for both spectra are identical. The number of samples is set to 10000 at a sampling interval of $1ns$ with a full range of $1 - 2V$. The peak detection and histogram parameters are varied to verify the most suitable settings.

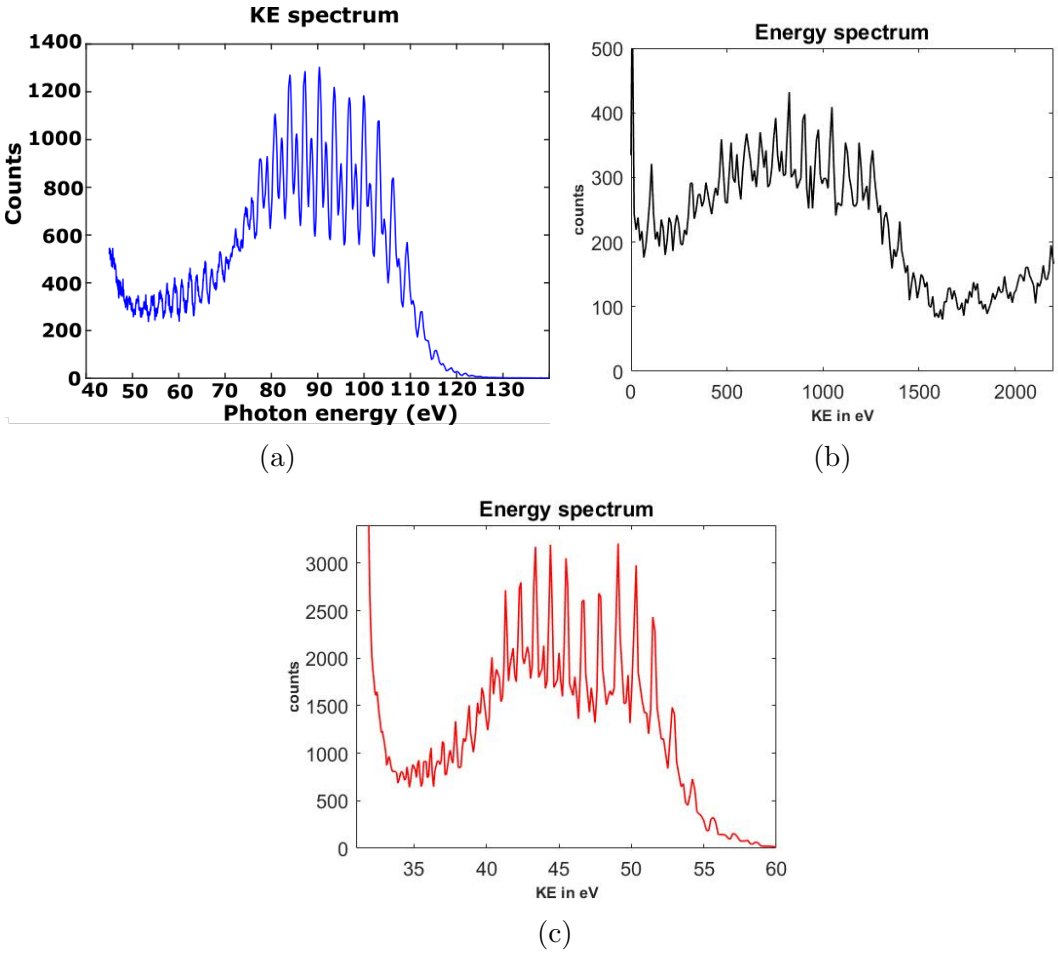


(a) (b) (c)

Figure 11: Kinetic energy spectra: (a) Energy spectrum acquired with the old fastcomtec DSPC (b) Energy spectrum measured with the new acquisition system U1084A corresponding to the TOF spectra in figure 10b (c) First energy spectrum acquired with the DSPC U1084A

The graphs above present the number of photoelectron counted per incoming photon energy in figure 11a and per kinetic electron energy in figure 11b and c. The peaks to construct the first spectrum in figure 11b are detected with a width value of 9

sample and the histogram is then built with 1000 bins of $5eV$ each. In figure 11a and b, the fact that the counts at low energy values approach infinity can be explained by photoelectron noise created in the TOF spectrum. For high TOF values, the number of counts is very low and possibly created by noise. During the TOF to KE conversion, these low counts are in the denominator thus create an infinite KE count. In order to avoid this noise signal, the photoelectron peaks can be collected when the laser is switched off and subtracted from the final measured peaks.

By comparing the energy axis in figure 11a and 11b, we can assume that the order of magnitude of the KE values in figure 11b is incorrect. This can be proven by comparing the energy states with the energy axis in figure 11b. However, one should note that figure 11a displays the photoelectron counts against the photon energy while figure b and c are kinetic energy spectra. As the laser resonance frequency corresponds to an energy of approximately $E_{omega} = \hbar\omega = \hbar\frac{2\pi c}{\lambda} = 1.55eV$ and the first ionization energy of neon is $E_{int} = 15.76eV$ [26], the energy at which the photoelectron peaks should appear can be estimated. Given that $\frac{E_{int}}{E_{omega}} \approx 10.2$, the $11th$ or at least the $13th$ harmonic should appear in the spectrum. As displayed in the method part 2.1.2 for the RABBITT technique, the photoelectron energy between two peaks induced by the $(2N+1)$th and $(2N+3)$th odd harmonics would correspond to a separation of roughly $3eV$ in this case which does not correspond to the displayed values in figure 11a and c.

After a verification of units, we found that part of the error in the energy conversion was made due to an inaccurate choice of mass units for $m_e$ in equation 8. When the mass is expressed in $MeV/c^2$ and the length L of the MBES tube is given by $3m$, the values on the energy axis are modified to an appropriate order of magnitude of $10^2\,eV$. However, the separation between the photoelectron peaks does still not correspond to $3\,eV$. As the TOF values measured by the $U1084A$ system correspond to the reference values provided by the old card, the offset in kinetic energy values is most likely not created by the energy conversion, but rather when the histogram is established. The limits of the histogram axis could have been chosen inaccurately and it should be reviewed how the energies are categorized into histogram bins. In the near future, we intend to correct and remove this error. During the experiment, it was not possible to create new spectra to verify the conversion procedure from TOF to kinetic energy. It is therefore important to save the raw data event per event to avoid the loss of information and to process data offline the running labview program.

## 3.4 Duty cycle

After the first trigger is corrected and the resolution is studied, the TOF and KE spectra now resolve the sideband signals as can be seen in figure 10a and 11c. They approach the shape of the spectra from the former card in figure 10a and 11a. However, by measuring the acquisition time, we found that the statistics of photoelectron peak counts in figure

10a and 11c only lie by 50% of the counts collected with the old card. In other words, at the moment the ratio between the time spent on accumulating data and the acquisition window (duty cycle [27]) is 0.5. However, for high reptition rate measurements, this ratio should be 1.

The remaining minor difference in resolution relative to the fastcomtec card has a software origin and most probably lies in the choice of a modular algorithm architecture and local variables of labview. Additionally, the labview peak detection manages high data sets. Since all acquisition and processing steps are executed sequentially in time, the management of these data sets is likely to slow down the acquisition speed.

There are three potential solutions for this problem. First of all, the high speed acquisition of the card has so far not been exploited which could be done by applying the Zero-Suppress mode. Furthermore, one should consider to reduce the use of local variables and to implement more parallelizing steps in the application software program. If those steps do not fulfill the desired duty cycle, the acquisition can be programmed with the C++ computer language instead [21]. At high repetition rates, an option is to measure photoelectron peaks after a number N of trigger events as the photoionization statistics are increased. In that case, the problem of missing out 50% of the data would be solved. However this approach significantly increases the data array and therefore the zero-suppress mode is critically needed.

At the moment, it is possible to acquire photoelectron spectra with the acquisition mode 0. The Zero-Suppress mode should allow to improve the situation in many ways , especially for high repetition rate measurement, since most of the hardware will do the work by reducing the amount of data sent to Labview and doing part of the peak detection work. So far this mode is configured and allows already to accumulate data. However, the threshold configuration still needs to be debugged, but it is understood how data can be divided into memory segments which are characterized by repetitive data structures.

# 4 Conclusion and Outlook

The initial motivation of this thesis is to generate higher-harmonics with the megahertz (MHz) Laser system in the Laser facility in Lund and to detect the induced photoelectron signal with a magnetic bottle electron spectrometer (MBES). The measurements were taken with an alternative femtosecond Laser in the attosecond laboratory which works at a repetition rate of $1kHz$ and the resulting pulses were detected with the there placed MBES. Although no measurements at high-repetition rates could be taken, the analysis of the detection tools and results is done with regards to future experiments in the MHz laboratory.

For the purpose of measuring high repetition rate spectra, during the thesis, the high speed acquisition card $U1084A$ hardware has been installed, implemented and an application software has been programmed. The analysis has shown whether the acquisition card with the programmed software can potentially acquire pulses incident at high repetition rate. The conclusion is that measurements at high-repetition rate measurement with the $U1084A$ card are possible, however some modifications to the software need to made and the cards functionalities such as the Zero-Suppress mode need to be exploited.

During the thesis a lot of time was spent with trial and error experiments of the card and the hardware installation as the documentation of labview driver functions provided was limited. The results and analysis have shown that an option to save raw data and to process it offline should be implemented. This will be useful to verify the TOF to energy conversion, to test histogram settings with identical raw data and simply to conserve the information of all photoionization processes. This information is needed later on to investigate coincidence measurements.

Secondly, the acquisition system needs to be improved to obtain a duty cycle of 100% at both 1 and 200 kHz. This can on the one hand be established on the hardware level by using the Zero-Suppress mode together with sequential acquisition settings [16]. On the other hand, the application software can be enhanced by using less local variables and implementing a different algorithm architecture. Moreover, another method to detect the photoelectron pulses in the raw data can be tested and compared to the current peak detection. If those methods do not improve the acquisition speed, another software environment might be more suitable for the high-speed measurements at $5\mu s$ rates and an alternative program could be chosen.

While on the one hand high repetition rate measurements try to reduce space-charge effects, it could on the other hand be interesting to study them and fundamentally understand how they behave.

In the long term, the acquisition system with the DSPC $U1084A$ can be further developed to measure the photoemission delay at high repetition rates, to perform coincidence measurements and study material disintegrations and to eventually increase the number of research work performed due to increased statistics.

# Appendix A Card installation

The following pictures show how the $U1084A$ card is installed in the computer number *atto*53 in the attolab at the atomic physics division.

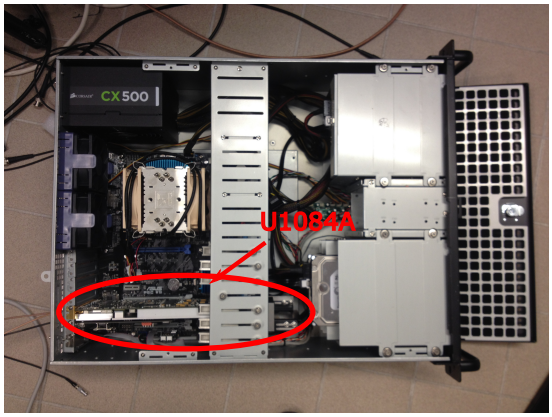


(a) Card placement in the lower left corner of the atto53 computer

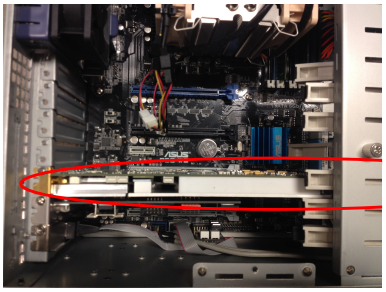

(b) Zoom into card installation

Figure A12: Pictures showing the digitizer card installed on the circuit board connected to a PCIe connection

Once the card is installed, its in- and outputs can be reached from the back of the computer.

# Appendix B MBES detector apparatus

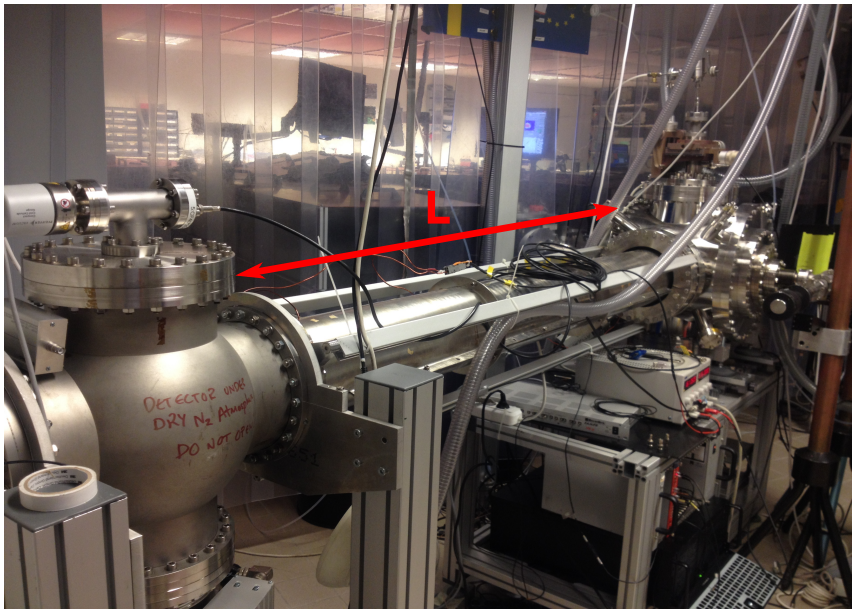


Figure B13: MBES apparatus of length L with the MCP plates

# Appendix C Labview software

The language used to program the application software in this thesis is Labview 2015 32-bit provided by National Instruments. Labview is a graphical software program which consists of two main parts: When a new file - virtual instrument (VI) in Labview - is opened, a front panel and a block diagram. The algorithm is programmed on the block diagram by using labview functions which can be opened by a right click on the block diagram (see figure below)and wires which connect the functions and indicate the logical data flow.

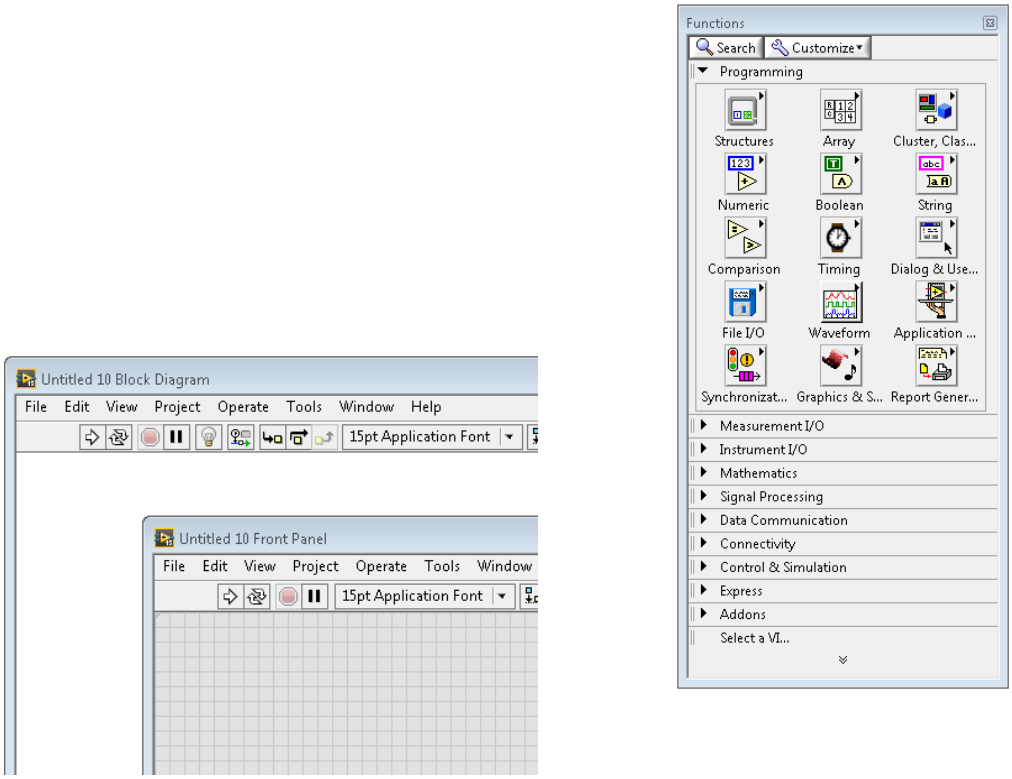


(a) Block diagram and front panel window of an untitled VI

(b) Function palette opened by a right click in the block diagram

Figure C14: Main features of Labview. Source: Labview 2015 32-bit Software by 2017 National Instruments Corporation.

The driver functions provided by keysight technologies are all defined in a dynamic link library called dll. The library is stored on the internal hardware with the format abbreviation .dll. A dll is a compiled library of several functions which can be exported and used by different programs such as Labview [21]. The dll can be called by a "Call Library Function Node". The implemented function out of the dll is defined under "function name", the data format is defined to be either the value or the pointer to an address and the input and output variables are linked to the corresponding cases of the "Node".

# Appendix D Application software

## D.1 Front panel

The front panel of the AP is mainly divided into two parts. The main tab is used for the cards settings and to visualize the data whereas the second tab is used to process data and plot the histograms.

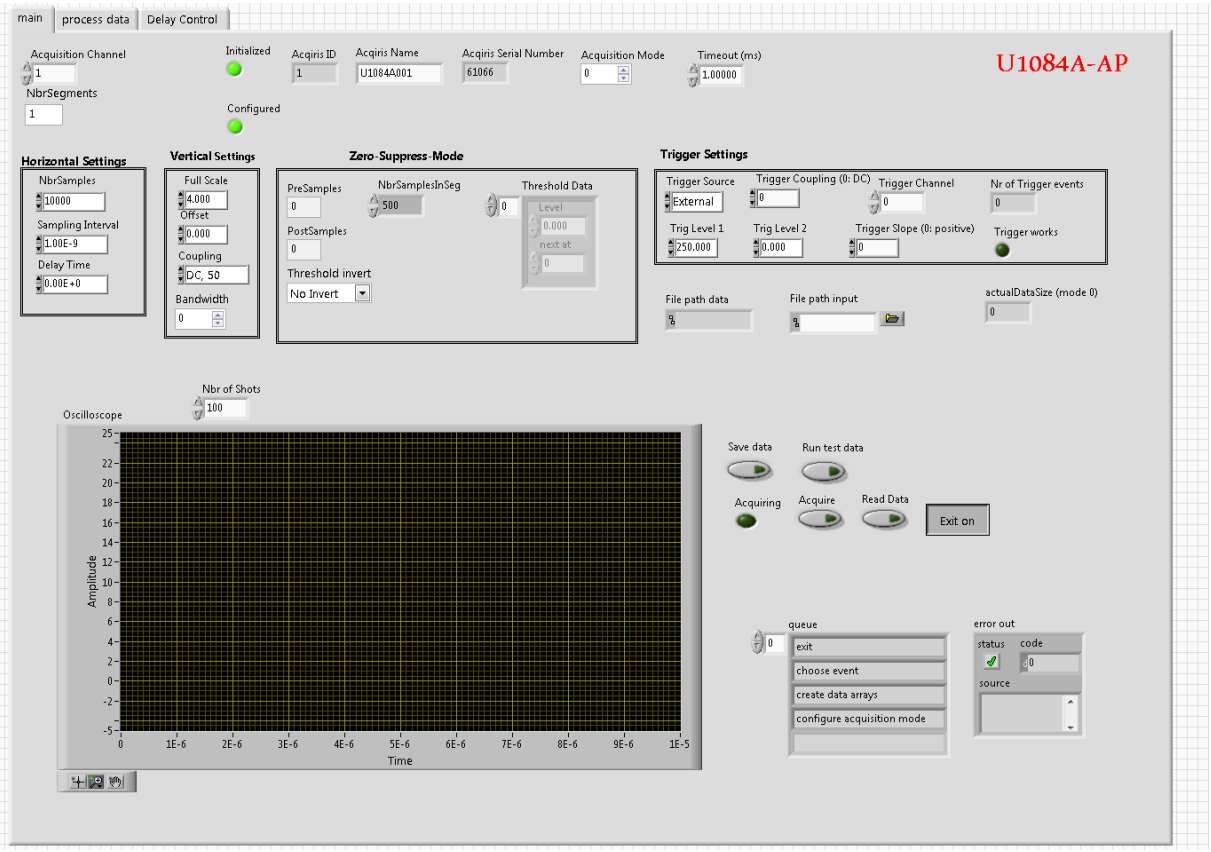


Figure D15: Front panel of the programmed application software with graphical window, settings and a "process" data tab

## D.2 Block diagram

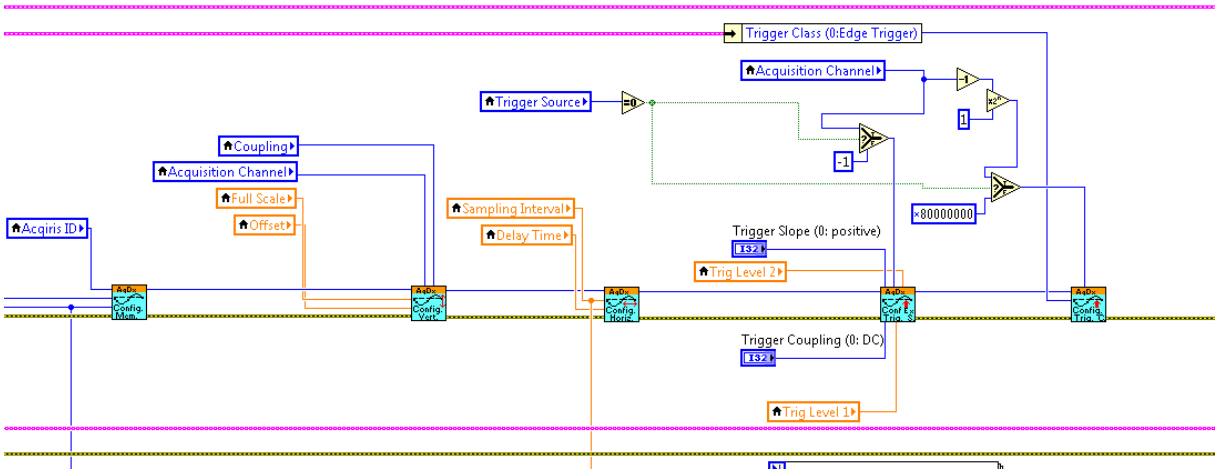


Figure D16: Function palette opened by a right click in the block diagram

The algorithm created in the block diagram is based on a case structure (see [21]). Each case is named by a string which corresponds to the algorithm steps enclosed in the case. The order at which the cases are executed is determined by a so-called event structure. An event corresponds to a change in the values of the front panel controls or the change in the boolean expression of a switch. For every defined event a number of cases are executed. If no event occurs, a timeout case is defined.

# Appendix E Matlab processing code

```
close all;
clear all;

histogram_new = fileread('TOFhisto16h42.txt');
output = textscan(histogram_new, '%f %d');

time_n = output{1}.';
counts_n = output{2}.';
counts_n = double(counts_n);

xmin =0;
xmax=5;
ymin=0;
ymax=1200;
```

```
[peaks, location, width, prominescence] = findpeaks(counts_n);
figure(1);
plot(time_n,counts_n,'-r','LineWidth',1.2,'Color',[1 0.5 0]);
set(gca,'fontsize',15);
xlim([xmin xmax]);
ylim([ymin ymax]);
xlabel('TOF in seconds','FontSize',12,'FontWeight', 'bold');
ylabel('counts','FontSize',12,'FontWeight', 'bold');
title('Time-of-flight spectrum');

figure(2)
findpeaks(counts_n);
xlim([0 5000]);
xlabel('Histogram Bin Number');
ylabel('Counts');
title('peak detection');
```

# References


[1] A. Verna et al. Space-charge effects in high-energy photoemission. *Journal of electron spectroscopy and related phenomena*, 209:14, 2016.

[2] P.M. Paul, E.S. Toma, P. Breger, G. Mullot, F. Augé, Ph. Balcou, H.G. Muller, and P. Agostini. Observation of a train of attosecond pulses from high harmonic generation. *Science*, 292:1689, 2001.

[3] M.Hentschel et al. Attosecond metrology. *Nature*, 414:509, 2001.

[4] P. Johnsson. *Attosecond optical and electronic wave packets.* PhD thesis, Lund University - Faculty of Engineering, 2002.

[5] J. Gagnon et al. *Attosecond Electron Spectroscopy: Theory and its applications.* PhD thesis, Ludwig-Maximilians-Universität München, 2010.

[6] J.M.Dahlström et al. Theory of attosecond delays in laser-assisted photoionization. *Chemical Physics*, 414, 2013.

[7] F. Calegari et al. Advances in attosecond science. *Journal of Physics B: Atomic, Molecular and Optical Physic*, 49, 2016.

[8] Ferec Krausz and Misha Ivanov. Attosecond physics. *Reviews of modern physics*, 81, 2009.

[9] V. Schmidt. Photoionization of atoms using synchrotron radiation. *Rep. Prog. Phys.*, 55:1483, 1992.

[10] A. Einstein. Über einen die erzeugung und verwandlung des lichtes betreffenden heuristischen gesichtspunkt. *Annalen der Physik*, 322, Nr. 6, 1905.

[11] J.Wätzel and A.S.Moskalenko. Angular resolved time delay in photoemission. *Journal of Physics B: Atomic, molecular and optical physics*, 48, 2015.

[12] P.Hockett et al. Time delay in molecular photoionization. *Journal of Physics B: Atomic, molecular and optical physics*, 49, 2016.

[13] Hans Jakob Wörner. Advanced kinetics, 2017.

[14] D. Guénot. *Probing electron correlation on the attosecond timescale.* PhD thesis, Lund University - Faculty of Engineering, 2014.

[15] C. M. Heyl et al. High-order harmonic generation with micro joule laser pulses at high repetition rates. *Journal of Physics B: Atomic, molecular and optical physics*, 45, 2012.

[16] Agilent Technologies, US. *Agilent U1084A*, 2012.

[17] Helena Jelinkova. *Laser for medical applications: Diagnostics, Therapy and Surgery*, volume 1. Woodhead Publishing, 2013.

[18] D. Kroon. *Attosecond interferometry: techniques and spectroscopy*. PhD thesis, Lund University - Faculty of Engineering, 2016.

[19] D. Samm. *1.4 Der NIM Standard*.

[20] Agilent technologies. *Programmer's guide Agilent Acqiris Instruments U1092-90003*. Agilent Technologies, April 2012.

[21] Jim Kring Jeffrey Travis. *LabVIEW for Everyone*, volume 3. Prentice Hall, 2008.

[22] Benedetta Viti. Zero suppress mode, aka threshold gating?

[23] 2017 National Instrument Corporation. Extending virtual memory usage for 32-bit windows.

[24] Armin Scrinzi Vinay Pramod Majety. Photo-ionization of noble gases: A demonstration of hybrid coupled channels approach. *Photonics*, 2, 2015.

[25] Agilent technologies. *Programmer's Reference Manual: Agilent Acqiris Instruments*. Agilent Technologies.

[26] Albert C. Thompson. *X-ray data booklet*, volume 3rd. Lawrence Berkeley National Laboratory.

[27] Pawel L. Urban. *Time resolved mass spectroscopy: from concept to applications*, volume 1st. Wiley.